

## A Simple Controlled Salt Decomposition Route to Synthesize Nanoporous Mn<sub>2</sub>O<sub>3</sub> Materials with Tunable Pore Structure and Narrow Pore Distribution

Chichao Yu, Jianlin Shi,\* and Dongsheng Yan

State Key Lab of High Performance and Superfine Microstructure, Shanghai Institute of Ceramics, Chinese Academy of Science, 1295 Ding-xi Road, Shanghai 200050, P. R. China

(Received September 18, 2007; CL-071024; E-mail: jlshi@sunm.shcnc.ac.cn)

A facile and novel method has been developed for synthesizing nanoporous Mn<sub>2</sub>O<sub>3</sub> materials with polyhedron morphology, high surface area, and narrow pore distribution by controlled thermal decomposition of the oxalate salt precursor. This method can be extended to the preparation of other kinds of nanoporous oxides.

Porous transition-metal oxides are interesting materials owing to their specific properties and diversity of structure and, therefore, have potentials in many applications. Because of the excellent cation exchange and molecular adsorptive properties of microporous metal oxides, they can be extensively used as ion sieves,<sup>1</sup> molecular sieves,<sup>2</sup> catalysts,<sup>3</sup> and so on. The outstanding electrochemical and magnetic properties of manganese oxides are also attracting for applications in rechargeable batteries<sup>4</sup> and new magnetic devices.<sup>5</sup> Porous manganese oxides are usually prepared mainly via two kinds of template method: surfactant as soft template<sup>6</sup> and mesoporous oxides (typically SBA-15) as hard template.<sup>7</sup> However, soft template method would introduce other cations into manganese oxide tunnels during processing, and hard template method usually produces porous manganese oxides with uncontrolled pore size and/or scattered pore size distribution. Some literatures have reported the synthesis of porous Mn<sub>2</sub>O<sub>3</sub> without template;<sup>8</sup> however, data of surface area and pore distribution were not given.

In this study, we report a simple template-free method to synthesize microporous and mesoporous Mn<sub>2</sub>O<sub>3</sub> materials with high surface area, narrow pore distribution and polyhedron morphology. In such an approach, nanopores are generated simply via the thermal decomposition of the salt anions from micrometer-sized particles, which is totally different from the mechanism of cooperative assembly from the starting molecular species with or without the presence of templates. This approach can be extended to other kinds of precursors and other kinds of nanoporous oxides. Nanoporous Mn<sub>2</sub>O<sub>3</sub> materials are obtained by decomposition of a manganese oxalate dihydrate precursor. A typical precipitation approach<sup>9</sup> is employed to prepare the precursor with controlled polyhedron morphology as follows: oxalic acid was added to an aqueous MnCl<sub>2</sub> solution in an oil bath, and dioctylsulfosuccinate (AOT) was used to control morphology of the precipitates. The subsequent thermal decomposition is conducted under a well-designed heating program. The samples are calcined at different temperatures in the air, and in this communication, we present the typical nanoporous manganese oxide samples calcined at 300 and at 400 °C (labeled as MO300 and MO400 in the following section).

Manganese is a transition element and has several different valences. XRD analysis together with XPS (X-ray photoelectron spectroscopy) are involved to investigate the chemical stoichi-

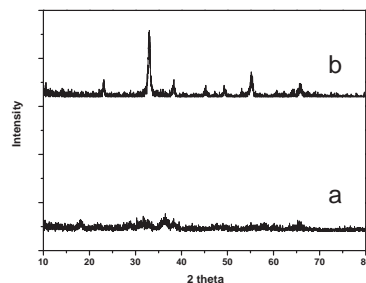


Figure 1. XRD patterns of the decomposed samples calcined at (a) 300 °C, (b) 400 °C.

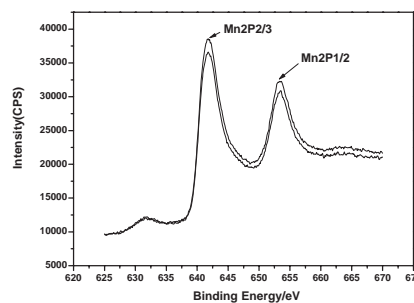
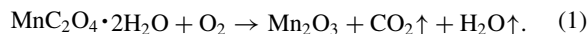


Figure 2. XPS spectra at Mn 2p<sub>3/2</sub> and Mn 2p<sub>1/2</sub> for samples prepared at 300 °C (upper) and 400 °C (lower).

ometry of the manganese oxide after decomposition and the valence of manganese (Figures 1 and 2). XRD analysis shows that samples calcined at 400 °C are well crystallized and can be identified as Mn<sub>2</sub>O<sub>3</sub> with body-centered cubic phase, whereas samples calcined at 300 °C are almost amorphous.

XPS spectra indicate that the Mn 2p<sub>3/2</sub> peak is centered at 641.8 eV and Mn 2p<sub>1/2</sub> peak at 653.3 eV, with a spin-energy separation of 11.5 eV which is in agreement with the reported data of Mn 2p<sub>3/2</sub> and Mn 2p<sub>1/2</sub> in Mn<sub>2</sub>O<sub>3</sub>.<sup>10</sup> The two samples calcined at different temperatures show the same peak positions of Mn 2p<sub>3/2</sub> and Mn 2p<sub>1/2</sub>. XPS and XRD results prove that these two samples calcined at different temperatures are both Mn<sub>2</sub>O<sub>3</sub>. The decomposition process undergoes the following reaction:



The total weight loss caused by gas bursting out is 55% or so in accordance with thermogravimetry (TG) result. Such high weight loss in calcined samples with limited shrinkage result in large amount of porosity remained within particles which can be observed at TEM images (Figure 3). Figure 3a shows the whole particle of MO300 with an octahedron morphology and homogeneous porosity. In Figure 3b, we can find out that those pores are randomly arranged but distributed homogeneous through out of the whole particle, but primary particles are

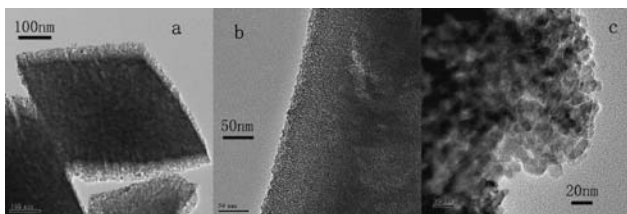


**Figure 3.** TEM images of MO300 (a) and (b), and MO400 (c).

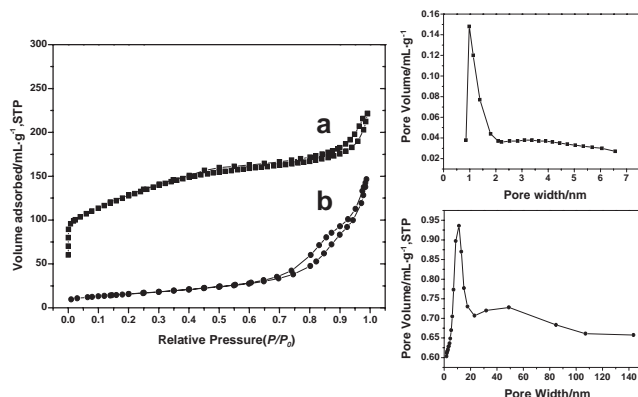


**Figure 4.** Nitrogen adsorption-desorption isotherm (left) at 77 K of MO300 (a), and MO400 (b) and pore distribution calculated from (up-right) curve a using Horvath-Kawazoe method, (lower-right) curve b using BJH method.

almost amorphous according to XRD and electron diffraction result (not shown). With elevating the heating temperature (Figure 3c), those primary particles start to crystallize and grow up (size increase from 3 nm in MO300 to 14 nm in MO400), while pores are also enlarged and the pore size distribution become scattered.

Nitrogen adsorption-desorption isotherm analysis (at 77 K) was employed for studying the pore structural properties (Figure 4). A steep uptake of N<sub>2</sub> at the very beginning of measurement ( $P/P_0 < 0.02$ ) (curve “a” in Figure 4) suggests that the prepared MO300 samples have micropores, which was obtained on a Micromeritics ASAP 2020 porosimeter for microporosity. However, the hysteresis loop of MO400 samples (obtained on a Micromeritics TriStar 3000 porosimeter for mesoporosity) beginning from 0.6 (curve “b” in Figure 4) shows that in MO400 samples micropores disappear and that pores evolve into mesoporous region. BET surface area of MO300 and MO400 samples are 283 and 56 m<sup>2</sup> g<sup>-1</sup>, respectively. The surface area of MO300 is significantly higher than porous manganese oxides prepared by hard template route (below 150 m<sup>2</sup> g<sup>-1</sup>).<sup>7</sup> Pore size distributions plots are also demonstrated in Figures 4, with that of MO400 being obtained by BJH method using the desorption branch of the isotherm and that of MO300 by Horvath-Kawazoe method<sup>11</sup> using the adsorption branch due to its micropore size. It is shown that MO300 have a rather steep distribution in 1 nm, and that of MO400 displays a narrow distribution in mesoporous region around 12 nm. So we can see that we are able to tune the pore size from the microporous to mesoporous region simply using a controlled thermal process. At relatively low

temperature of calcination (300 °C), CO<sub>2</sub> and CO are generated from manganese oxalate, while Mn<sub>2</sub>O<sub>3</sub> framework composed of very small primary particles and micropores are formed among the primary particles. At a higher temperature (400 °C), Mn<sub>2</sub>O<sub>3</sub> primary particles crystallize out as nuclei and quickly grow up into crystallites larger than 10 nm by adsorbing surrounding primary particles via Oswald ripening.<sup>12</sup> During this process, micropores among the amorphous primary particles evolve into mesopores among the crystallites.

The electrochemical properties of nanoporous Mn<sub>2</sub>O<sub>3</sub> are investigated by measuring the cyclic voltammograms of the samples. Specific capacitance of as high as 350 F/g is obtained for MO300, while that of MO400 drops to 66 F/g. So the specific capacitance is dependent on the surface area, and the microporous Mn<sub>2</sub>O<sub>3</sub> with high surface area is promising for application in supercapacitors.

In conclusion, we present a facile and novel method to synthesize nanoporous Mn<sub>2</sub>O<sub>3</sub> materials with high surface area and narrow pore distribution by controlling the thermal decomposition process. Pore size can be tuned from microporous region to mesoporous simply by a controlled thermal process. Microporous Mn<sub>2</sub>O<sub>3</sub> shows promising electrochemical properties for application in supercapacitors. This approach can be extended to other kinds of precursors and other kinds of nanoporous oxides.

The financial support of National Natural Science Foundation of China (Grant Nos. 20633090 and 50672115) and National Basic Research Project (No. 2002CB613300) is gratefully acknowledged.

## References

- Z. Liu, K. Ooi, *Chem. Mater.* **2003**, *15*, 3696.
- Y. F. Shen, R. P. Zerger, R. N. Deguzman, S. L. Suib, L. McCurdy, D. I. Potter, C. L. O'Young, *Science* **1993**, *260*, 511.
- H. Cao, S. L. Suib, *J. Am. Chem. Soc.* **1994**, *116*, 5334.
- A. R. Armstrong, P. G. Bruce, *Nature* **1996**, *397*, 53.
- S. Mori, C. H. Chen, S. W. Cheong, *Nature* **1998**, *392*, 473.
- a) B. Ammundsen, D. J. Jones, J. Roziere, G. R. Burns, *Chem. Mater.* **1996**, *8*, 2799. b) K. Ooi, Y. Miyai, S. Katoh, *Sep. Sci. Technol.* **1987**, *22*, 1779. c) P. Boullay, M. Hervieu, B. Raveau, *J. Solid State Chem.* **1997**, *132*, 239. d) S. Ching, J. L. Roark, N. Duan, S. L. Suib, *Chem. Mater.* **1997**, *9*, 750. e) C. S. Johnson, D. W. Dees, M. F. Mansuetto, M. M. Thackeray, D. R. Vissers, D. Argyriou, C.-K. Loong, L. Christensen, *J. Power Sources* **1997**, *68*, 570.
- H. Chen, X. Dong, J. Shi, J. Zhao, Z. Hua, J. Gao, M. Ruan, D. Yan, *J. Mater. Chem.* **2007**, *17*, 855.
- a) L.-X. Yang, Y.-J. Zhu, H. Tong, W.-W. Wang, *Ultrason. Sonochem.* **2007**, *14*, 259. b) Z. Yang, W. Zhang, Q. Wang, X. Song, Y. Qian, *Chem. Phys. Lett.* **2006**, *418*, 46.
- Z. A. D. Lethbridge, A. F. Congreve, E. Esslemont, A. M. Z. Slawin, P. Lightfoot, *J. Solid State Chem.* **2003**, *172*, 212.
- B. J. Tan, K. J. Klabunde, P. M. A. Sherwood, *J. Am. Chem. Soc.* **1991**, *113*, 855.
- S. U. Rege, R. T. Yang, *AIChE J.* **2000**, *46*, 734.
- H. C. Zeng, *J. Mater. Chem.* **2006**, *16*, 649.